Published in final edited form as:

Mol Cancer Res. 2020 March ; 18(3): 364–374. doi:10.1158/1541-7786.MCR-19-0764.

Bayesian modeling identifies PLAG1 as a key regulator of proliferation and survival in rhabdomyosarcoma cells

Yanbin Zheng[1,4], **Lin Xu**[1,2,4], **Mohammed Hassan**[1], **Xiaoyun Zhou**[1], **Qinbo Zhou**[2], **Dinesh Rakheja**[3,4], **Stephen X. Skapek**[1,4,5]

[1]Department of Pediatrics, Division of Hematology/Oncology, University of Texas Southwestern Medical Center, Dallas, TX

[2]Quantitative Biomedical Research Center, Department of Population & Data Sciences, University of Texas Southwestern Medical Center, Dallas, TX

[3]Department of Pathology, University of Texas Southwestern Medical Center, Dallas, TX

[4]Harold C. Simmons Comprehensive Cancer Center, University of Texas Southwestern Medical Center, Dallas, TX

[5]Gill Center for Cancer and Blood Disorders, Children's Health Children's Medical Center, Dallas, TX

Abstract

We recently developed a novel computational algorithm that incorporates Bayesian methodology to identify rhabdomyosarcoma (RMS) disease genes whose expression level correlates with copy-number variations, and we identified *PLAG1* as a candidate oncogenic driver. Although PLAG1 has been shown to contribute to other type of cancers, its role in RMS has not been elucidated. We observed that PLAG1 mRNA is highly expressed in RMS and is associated with *PLAG1* gene copy-number gain. Knockdown of PLAG1 dramatically decreased cell accumulation and induced apoptosis in RMS cells, whereas its ectopic expression increased cell accumulation *in vitro* and as a xenograft and promoted G_1 to S phase cell cycle progression. We found that PLAG1 regulates IGF2 expression and influences AKT and MAPK pathways in RMS, and IGF2 partially rescues cell death triggered by PLAG1 knockdown. The expression level of PLAG1 correlated with the IC_{50} of RMS cells to BMS754807, an IGF receptor inhibitor.

Keywords

rhabdomyosarcoma; PLAG1; IGF2; proliferation; survival

Corresponding Authors: Yanbin Zheng, PhD (Yanbin.Zheng@UTSouthwestern.edu), Stephen X. Skapek, MD (Stephen.Skapek@UTSouthwestern.edu), UT Southwestern Medical Center, 5323 Harry Hines Blvd, Dallas, TX 75390. Phone: 214-648-3081; Fax: 214-648-3122.

The authors declare no potential conflicts of interest.

Introduction

Rhabdomyosarcoma (RMS) is the most common soft tissue sarcoma in children (1,2). Histologically, it can be classified into two major types: embryonal RMS (ERMS) and alveolar rhabdomyosarcoma (ARMS) (3-5), with the majority of ARMS containing PAX3-FOXO1 or PAX7-FOXO1 fusion genes (6). Recent next-generation sequencing studies have advanced our knowledge of RMS biology. Somatic single nucleotide variants (SNVs) have been identified primarily in the fusion-negative (FN) forms of RMS; recurrently mutated genes include *NRAS*, *KRAS*, *HRAS*, *PIK3CA*, *FGFR4*, *FBXW7*, *CTNNB1*, *BCOR*, *NF1*, and *P53* (7-9). The recurrence of these mutations across RMS is relatively low, with exception of the RAS family which are mutated in approximately 25% of FN-RMS cases (7,8). Beyond individual genes, work from the Khan laboratory shows that 93% of FN-RMS samples have alterations in receptor tyrosine kinase (RTK)/PI3K or RAS/MAPK pathways, including IGF2 and IGF1R (8).

Although the vast majority of SNVs show little recurrence across RMS specimens, gene copy-number changes are very common and more highly recurrent. To gain a better understanding of those that may serve as oncogenic drivers or tumor suppressors, we recently developed a Bayesian-based computational algorithm for integrative analysis of gene expression and copy-number (10). The so-called iExCN algorithm identified 25 candidate oncogenic drivers based on gene copy-number/expression gains in FN-RMS, and close to half of those were functionally validated in cultured RMS lines (10). One of those candidate drivers is *PLAG1*, which is of particularly interest given the growing understanding of the importance of RTK/PI3K/MAPK pathway activation in this disease. The oncogenic capacity of *PLAG1* was first described in pleomorphic adenoma of the salivary gland (11), and later in lipoblastoma (12), hepatoblastoma (13), acute myeloid leukemia (14) and Wilms tumor (15). In some of these cases, elevated expression of PLAG1 mRNA and protein was attributed to chromosomal translocation placing *PLAG1* expression under the control of an active promoter, such as *CTNNB1* (11), *LIFR* (16) or *TCEA1* (17) in pleomorphic adenoma of the salivary gland, and *HAS2* or *COL1A2* in lipoblastoma (18). That mechanism of activation contrasts how we found *PLAG1*, which was based on coupled gene copy-number and expression gains (10).

PLAG1 is the prototypical member of a small gene family that encodes a C2H2 zinc finger transcription factor (11). Initial functional studies focused on identifying a consensus DNA binding element (a core sequence GRGGC followed by a GGG cluster (19)); and transcriptional targets include a number of growth factors, such as IGF2 (19,20). Knockout of mouse *Plag1* allows viable offspring, but they display a major phenotype of smaller body size, beginning in later stages of embryonic development and persisting with age (21). Importantly, even though *Igf2*-deficient mice have growth retardation similar to the $Plag^{-/-}$ embryos (22), the *Plag1* knockout mice are reported to have normal *Igf2* expression (21). Importantly, mouse (and human) Plag1 expression is largely extinguished beyond the embryonic period (11,21,23).

Given the importance of mammalian *PLAG1* in embryonic growth, its normal silencing in the postnatal period, and direct connections to IGF2, well-known to influence RMS biology

(24,25), we carried out functional and mechanistic studies of how PLAG1 influences RMS cells *in vitro* and in xenograft models. Our findings implicate it as a survival factor that at least partially depends on IGF2, and expression of PLAG1 may be a determinant of relative sensitivity to targeted therapies focused on IGF2.

Materials and Methods

Cell lines, reagents and RMS tumor specimens

RMS cell lines RD, RD-like, RH30, RH18, and RH28, either provided by P. Houghton (St. Jude Children's Research Hospital) or obtained from ATCC, were cultivated in DMEM supplemented with 10% FBS, penicillin/streptomycin, and glutamine. All cells were authenticated by short tandem repeat (STR) testing and maintained *Mycoplasma*-free. RD-like cells have similar Short Tandem Repeat (STR) features with RD cells, but different gene expression and mutation profiles, and therefore likely represent a divergent sub-line (LX and SXS, unpublished).

Archived pathology specimens were obtained from the pathology laboratory at Children's Health Children's Medical Center (CMC) at Dallas, and the use of these deidentified cases was approved by the UT Southwestern Medical Center Institutional Review Board, which governs research work accomplished in partnership with CMC Dallas. All research involving animals was conducted according to protocols approved by the UT Southwestern Medical Center Institutional Animal Care and Use Committee (IACUC).

Manipulating PLAG1 expression

PLAG1 expression plasmid (EX-Z6241-Lv201) was purchased from GeneCopoeia, Inc. In this expression plasmid, PLAG1 is under the control CMV promoter and GFP is co-expressed under the control of SV40 promoter. Coding sequence of PLAG1 has been confirmed by Sanger sequencing. Lentivirus was produced by co-transfecting HEK293 cells with the PLAG1 expression vector (or control vector), psPAX2, and pMD2.G. The supernatants were collected at 48 and 72 hours, pooled, filtered with 0.45 μM filter, split into aliquots, stored at −80°C, and used later to infect cells. PLAG1 expression was diminished by transient knockdown using siRNA, essentially as previously described (26,27). The siRNA duplexes targeting *PLAG1* were purchased from Sigma with ID number of SASI_Hs01_00155522 and SASI_Hs01_00155525 (#2). Lipofectamine RNAiMAX was obtained from Thermo Fisher Scientific.

Measuring cell cycle, apoptosis, and cell accumulation

Cell cycle status and apoptosis was assessed in experimentally manipulated RMS cells using standard approaches. For cell cycle distribution, attached and floating cells were harvested and stained with propidium iodide (1 mg/ml) (Sigma-Aldrich). Cell proliferation was also assessed in RMS xenografts using immunostaining for Ki67 (BD Pharmingen, catalog # 556003) as previously described (28).

Apoptosis was measured using the BD Pharmingen Apoptosis, DNA Damage and Cell Proliferation kit (51-9007685AK), according to the manufacturer's instructions. Briefly,

cells were fixed and permeabilized with BD solution, treated with DNase, and stained with PE anti-cleaved PARP1 (Asp214) conjugated antibody. In all cases, stained cells were analyzed by FACS using BD FACSCalibur using FlowJo software.

Cell accumulation was measured using CyQUANT Cell Proliferation Assays Kit (Thermo Fisher Scientific) according to the manufacturer's instructions. Briefly, 1×10^3 cells were seeded in each well of 96-well plates with 6 replicates. Cells were refed at 3 days and harvested at 6 days.

RNA and protein expression

RNA expression was assessed by real-time quantitative (q) RT-PCR, essentially as previously described (29) using KAPA SYBR FAST qPCR kits (Kapa Biosystems) and the CFX96 Real Time System (Bio-Rad). Primers for qRT-PCR were as follows: *PLAG1:* 5'-GAG GGA GGA TGT TAA AGC CC −3' (sense), 5'- GCT CCA AAC TCT AGC AAG GC −3' (antisense); *IGF2:* 5'- AGA AGC ACC AGC ATC GAC TT −3' (sense), 5'- GCT GGC AGA GGA GTG TCC −3' (antisense); *GAPDH:* 5'- GAA GGT GAA GGT CGG AGT CA −3' (sense), 5'- TTG AGG TCA ATG AAG GGG TC −3' (antisense).

Protein expression was assessed by western blotting and immunohistochemistry as previously described (27). For western blotting, the following antibodies were used to measure: HSC70 (loading control, catalog # 7298, Santa Cruz Biotechnology); PLAG1 (catalog # WH0005324M2, Sigma-Aldrich); IGF2 (catalog # ABC504, EMD Millipore); phospho-AKT (catalog # 9271), AKT (catalog # 4691), phospho-p44/p42 MAPK (catalog # 9101), p44/p42 MAPK (catalog # 9102), phospho-IGF1R (catalog # 3918) and IGF1R (catalog # 3018), all from Cell Signaling Technology. PLAG1 protein expression in three formalin-fixed, paraffin-embedded FN-RMS tissue specimens was assessed by **i**mmunohistochemical staining using a PLAG1-specific antibody (SAB4301853, Sigma-Aldrich) with the Dako Omnis autostainer with heat-induced epitope retrieval at high pH, standard immunoperoxidase techniques, and hematoxylin counterstain. Digital images were captured with an Olympus DP21 camera. The intensity of IHC staining was scored from 0 to 3 (0 – no staining, 1 – mild staining, 2 – moderate staining, 3 – strong staining). The percentage of cells showing nuclear staining was scored from 0 to 3 (0 – no staining, 1 – >0, <10%, 2 – 10-50%, 3 – >50%). The final IHC score, shown with each photomicrograph, was calculated by multiplying the intensity score with the percentage positivity score (range 0 to 9).

Xenograft models

For *in vivo* tumorigenesis assay, 7×10^6 RH28 cells transduced with lentiviral expression vectors for *GFP* or *PLAG1-GFP* were resuspended in PBS and matrigel (1:1 ratio), and injected subcutaneously in the unilateral flank of NOD/SCID mice purchased from the UTSW breeding core (8-12 weeks old, 5 animals/group). Tumor size was measured 2-3 times per week by calipers, and volume was calculated with the formula: volume = $[(\text{width})^2 \times \text{length}]/2$ where width was the smallest of 2 measurements. Endpoint tumor size was adopted at 2.0 cm^3. All mice bearing either *GFP* or *PLAG1-GFP* tumors were euthanized by CO_2 at the same time once the largest tumor reached 2.0 cm^3.

Xenografted tissue was harvested from euthanized mice and fixed for 24 hours in 4% paraformaldehyde (PFA) in PBS and processed for paraffin-embedded sections. Routine H&E was performed as previously described (28-30). Cell proliferation was assessed by staining with anti-Ki67 primary antibody followed by biotinylated secondary antibody (Universal Antibody), which was detected by using DAB Peroxidase (HRP) Substrate Kit (with Nickle), 3'3-diaminobenzidine (Vector Laboratories). Cell apoptosis was assessed by terminal deoxynucleotidyl transferase (TdT)-mediated dUTP nick end labeling (TUNEL) using the In Situ Cell death Detection kit, POD (Roche). Ki67- and TUNEL-positive cells were calculated as a percentage of the total number of cells, which was determined from hematoxylin counterstain. Staining was quantified using representative sections of the tumor taken from each of 4 animals each bearing xenografted cells expressing either GFP or PLAG1/GFP. Digital photomicrograph images (40X magnification) were captured from a non-necrotic area of the tumor and without knowledge of whether the tumor cells expressed GFP or PLAG1/GFP. Image J software was utilized to quantify positively stained nuclei in each field, and that number was expressed relative to total cell number.

Bioinformatics and statistical analyses

RNA-seq data from 42 RMS tumors was downloaded from The European Genome-phenome Archive (EGA) with accession number EGAD00001000878. Gene copy-number and expression data analysis was described previously (10). Laboratory-based quantitative data are presented as a mean with standard deviation from multiple representative experiments. Statistical significance (P value < 0.05) was calculated using the unpaired Student's t-test and other tests as indicated in the main text or Figure legends.

Results

PLAG1 expression correlates with gene copy-number gain

Recently, the iExCN analysis pipeline identified *PLAG1* as a candidate oncogenic driver in RMS but its functional importance was not confirmed using a CRISPR/Cas9 mini-pool screen in two RMS cell lines (10). Given its known role as an oncogene in other tissues, we nevertheless explored its possible importance in more detail. First, using RNAseq data from a panel of 42 RMS specimens, we demonstrated PLAG1 expression to be elevated (FPKM>1) in 57% (24/42) of RMS specimens (Figure 1A), and it was particularly enriched in fusion negative (FN) cases (79%, 23 of 29) versus those positive for a PAX3 (or PAX7)-FOXO1 fusion (8%, 1 of 13) (two-tailed P value < 0.0001, Fisher's exact test). Average expression of PLAG1 mRNA expression was also higher in FN versus FP specimens (Figure 1B). Increased *PLAG1* gene copy-number correlated with higher PLAG1 expression (Figure 1C), a finding that is consistent with predictions from the iExCN pipeline (10). Immunohistochemical staining of three FN RMS specimens confirmed that PLAG1 protein was localized to the nucleus, consistent with its known role as a transcription factor (Figure 1D). The staining score of the specimens varied from 3 to 9 (9 is the highest), consistent with the varying but elevated mRNA expression of PLAG1 in many FN RMS specimens (Figure 1A). These data all support the premise that PLAG1 expression, driven by gene copy-number gains, might serve as an oncogenic driver in FN RMS.

PLAG1 can influence RMS survival by controlling IGF2 signaling

We extended these studies to cultured RMS models to begin to gain insights into mechanisms by which PLAG1 could act. Like human RMS specimens, PLAG1 expression varied at both RNA and protein level in a panel of five RMS cell lines (FN: RD, RD-like, RH18; FP: RH28, RH30). PLAG1 mRNA and protein were highest in RD, RD-like, and RH30, and much lower in RH18 and RH28 cells (Figure 2A and B). Focusing on the three lines with highest PLAG1 expression, we demonstrated that transient PLAG1 mRNA and protein knockdown significantly decreased cell accumulation at 6 days (Figure 2C and Supplementary Figure S1). Studying whether PLAG1 might control the cell proliferation cycle, we utilized flow cytometric analysis of propidium iodide (PI) -stained cells. Focusing on RD-like and RH30, lines that are most greatly compromised by PLAG1 knockdown, analysis of PI-stained cells showed marked increase in a sub-G_1 cell population with relatively small changes in the relative fraction in G_1 and G_2/M phases of the cell cycle (Figure 2D). To confirm that the increased sub-G_1 population was due to apoptosis, we demonstrated that PLAG1 knockdown increased the expression of cleaved PARP1 protein (Figure 2E and Supplementary Figure S2). Using an additional siRNA (#2), we consistently found that knockdown of PLAG1 significantly decreased cell accumulation, and increased the sub-G_1 population, a finding associated with increased expression of cleaved PARP1 in RD-like and RH30 cells (Supplementary Figure S3). These results indicate that PLAG1 supports RMS cell survival in cultured RMS cells.

Insulin-like growth factor (IGF) 2 is a well-recognized survival factor (31), and IGF2 is known to be a direct transcriptional target of PLAG1 (20). In cultured RMS cells, PLAG1 knockdown significantly decreased IGF2 expression, and in RH30 cells, the knockdown attenuated AKT and MAPK signaling, known to be downstream of IGF2 (32,33) (Figure 3A and B, Supplementary Figure S4). To prove a functional relationship between decreased IGF2 signaling and apoptosis induced by PLAG1 silencing, we demonstrated that exogenous IGF2 partially decreased the sub-G_1 cell population and partially restored AKT signaling that was attenuated by PLAG1 knockdown (Figure 3C, Supplementary Figure S5 and Supplementary Figure S6). Further, ectopic expression of PLAG1 in RH28 cells, a RMS line with relatively low PLAG1 (Figure 2A and B) increased IGF2 expression and its downstream signaling (Figure 3D and E, Supplementary Figure S7). Together, these data show that PLAG1 can contribute to survival of RMS cells at least partially by enhancing IGF2 expression and signaling in cultured RMS cells.

PLAG1 expression can influence response to IGF-1R inhibitor

Because PLAG1 controls IGF2 expression, we considered whether PLAG1 expression could influence response of RMS cells to the type 1 IGF receptor (IGF-1R) inhibitor, BMS754807 (34), which has been tested in clinical trials. We first determined the IC_{50} of BMS754807 in four different RMS cell lines, and we found a 100-fold difference in sensitivity to BMS754807 with RD being least and RH28 being most sensitive (Figure 4A). Interestingly, PLAG1 mRNA expression in the RMS cells positively correlated with the IC_{50} of BMS754807 in these cells (Figure 4B).

To further explore whether PLAG1 expression can serve as a biomarker for responsiveness to this inhibitor, we knocked down PLAG1 in RD cells, which have relatively high expression of that gene, and we ectopically expressed it in RH28 cells, which have relatively low expression. We found that PLAG1 silencing decreased the IC_{50} of BMS754807 to 40% of baseline (480 nM versus 1188 nM) and ectopic PLAG1 increased the IC_{50} by 2.6 fold (76 nM versus 29 nM) as compared to control (Figures 4C and D). In addition, BMS754807 treatment decreased phospho-IGF1R, phospho-AKT and phospho-MAPK without affecting the expression level of PLAG1 (Figure 4E and Supplementary Figure S8), consistent with it acting downstream of IGF2. BMS754807 treatment also significantly increased the sub-G_1 phase of cell cycle, similar to PLAG1 knockdown (Figure 4F). Unlike PLAG1 knockdown, though, IGF-1R inhibition also significantly increased the G_1 arrest in cultured RMS cells (Figure 4G). In summary, *PLAG1* expression may influence dependency on IGF-1R signaling in RMS.

PLAG1 drives excess proliferation in cells and tumor growth in xenograft

To test whether elevated PLAG1 expression can drive proliferation of RMS cells, we transduced RH28 cells (which have relatively low PLAG1 at baseline, Figure 2A and B) control lentivirus or lentivirus expressing PLAG1, and we measured relative accumulation *in vitro* and *in vivo*. Ectopic expression of PLAG1 in RH28 cells significantly increased cell accumulation *in vitro* (Figure 5A and B), and that correlated with an increased number of cells in S-phase of cell cycle (Figure 5C and D). Xenografts of PLAG1-expressing RH28 cells tended to be larger than those expressing the control GFP protein alone (Figure 5E); wet weight of dissected tumor was not available as a complementary assessment of size. Histological examination xenografted tumors showed features consistent with alveolar rhabdomyosarcoma in both GFP and PLAG1-expressing xenografts. Although we detected no significant difference in Ki67 staining, we detected significantly decreased TUNEL staining in PLAG1-expressing xenografts (Figure 5F-H). These results demonstrate that ectopic PLAG1 expression can hasten RMS cell proliferation *in vitro* and xenograft growth *in vivo*, and the latter may be driven by decreased baseline apoptosis.

Discussion

The application of molecular genetics and functional genomics tools has illuminated many elements of RMS biology (2). Fundamentally, RMS is divided into FP and FN disease, and those categories have distinct molecular features and clinical behavior (1-3,35). FP-RMS has a less favorable biology that requires more intensive therapy, but critical vulnerabilities stemming from that fusion protein are not yet clear, in part due to the paucity of targetable mutations associated with FP-RMS (2,8). In contrast, FN-RMS harbors activating mutations in *RAS* genes in approximately twenty-five percent of the cases (7,8). FN-RMS typically harbors a relatively large number of other genes with deleterious mutations; though the individual aberrations are rarely recurrent, computational analyses point to RTK/PI3K/MAPK pathways as being particularly important. Beyond the minority of cases harboring *RAS* or *PIK3CA* mutations and small fraction with mutations affecting an RTK (e.g., FGFR4), how deregulated RTK signaling is propelled has not been clear. Our findings indicate that PLAG1 can contribute to this deregulated RTK signaling. PLAG1 is frequently

expressed in FN-RMS specimens, and its expression correlates with gene copy-number gains – implying a "hard-wired" mechanism to sustain its expression. PLAG1 expression is generally low in FP RMS specimens which is consistent with our failure of finding copy number gain of *PLAG1* in FP RMS. Tumor-promoting effects of PLAG1 in RMS cells, including suppressing apoptosis, can be partly explained by its regulation of IGF2 and downstream signaling. But the partial correction of defects related to PLAG1 knockdown implies a role for other PLAG1 regulated genes. Exogenous PLAG1 in xenografted RMS cells hastens tumor formation in a manner that seems to correlate with decreased apoptosis within the growing tumor. We concede that the effects of ectopic PLAG1 on tumor size are relatively small. Moving forward, it will be important to further study its role in tumor growth using additional RMS models, including those in which endogenous PLAG1 is silenced.

Uncovering a role for PLAG1 in FN-RMS is particularly interesting because the IGF signaling pathway has been implicated in normal skeletal myogenesis and in rhabdomyosarcoma. Both IGF1 and IGF2 ligands are induced during myoblast differentiation *in vitro* (36,37), and ectopic expression of IGF1 and IGF2 in myoblasts or mice fosters muscle differentiation (38,39). Moreover, inactivation of either gene in the developing mouse leaves animals that are substantially smaller than wildtype controls (22,40). That IGFs also propel myoblast proliferation, a process that is exclusive of differentiation (41), seems to hinge on relative activation of p44/p42 MAPK-dependent pathway (42). This pathway is also implicated in the biology of both FP and FN-RMS. IGF-1R is a direct transcriptional target of the PAX3-FOXO1 fusion protein (43) and IGF2 is highly expressed in both FN and FP RMS. In some cases, including cases of FP RMS where *PLAG1* expression is low, increased IGF2 expression has been linked to loss of imprinting (LOI) and uniparental disomy [loss of heterozygosity (LOH)] (5,24,25). Pharmacological inhibition of MTOR1 using rapamycin leads to apoptosis, which is at least partially dependent on IGF-1R (44), and signaling through this receptor also limits cell death in RMS cells exposed to the chemotherapy agent cisplatin (45). Recognizing that PLAG1 copy-number gains correlate with increased expression of the protein and increased expression of IGF2 in cultured cells increases our understanding of one mechanism by which the pathway can be activated, especially in FN-RMS.

Where PLAG1 activity lies in the spectrum from initial rhabdomyosarcoma formation to progression and dissemination is not yet known. That primarily deregulated expression of PLAG1 could be an initiating event is supported first by the fact that a number of cancers are already associated with chromosomal translocations resulting in higher PLAG1 expression (11,18). Also, the Chen laboratory team recently showed that microRNA processing defects in Wilms tumor, another dysontogenic cancer in children, lead to elevated levels of PLAG1 (15). Though rare, FN-RMS is one of the childhood cancers associated with germline *DICER* mutations (46). Nevertheless, we identified PLAG1 as a candidate RMS driver based on coordinately elevated gene copy-number and expression in FN RMS but not in FP RMS (10), and the vast majority of the copy-number gains in FN-RMS are felt to represent somatic changes that accumulate during tumor formation/progression. Indeed, PLAG1 was only one among 25 iExCN-defined oncogenic drivers, and the number of iExCN genes harboring copy-number gains correlated with worse event-free and overall survival in two

different cohorts (10). This fact implies that the malignant behavior of FN-RMS is likely proscribed by multiple contributing factors. How deregulated *PLAG1* expression influences RMS formation or facets of tumor biology (e.g., progression, resistance to apoptosis) are tractable questions that can be addressed using available cell and organism-based models.

We have also considered the potential clinical translation of our findings, especially as they relate to therapeutically targeting the IGF signaling pathway. Much effort has been devoted to this in RMS but, for the most part, clinical trials have shown that IGF-1R inhibitors cixutumumab and R1507 have shown essentially no activity, even though the agents were well tolerated as single agents (47,48), or in combination with temsirolimus (49). The negative findings were surprising given that the drugs showed substantial activity in pre-clinical RMS models (50,51). There are many potential reasons for failure, including evolving resistance to IGF-1R inhibition. Based on our demonstrating that elevated expression of PLAG1 can significantly increase the IC_{50} of BMS-754807 in established RMS cells, that could also be considered as a possible resistance mechanism. The clinical trials could also have failed because the IGF pathway may only be a vulnerability in a subset of FN-RMS cases. Given the complexity of the biology of IGF ligand mRNA and protein processing and signal transduction, IGF expression is not likely to present a useful molecular biomarker to predict response to IGF pathway inhibitors. Coordinately elevated *PLAG1* gene copy-number and expression could represent a feature that is hard-wired into the genome during tumor formation/progression, as a more stable biomarker for targeting signaling through IGF2. Of note, other transcriptional targets for PLAG1 include cytokine-like factor-1 (CLF-1), placental growth factor (PIGF) or vascular endothelial growth factor (VEGF) (20,52) may also contribute to RMS. The development of increasingly sophisticated patient-derived RMS xenograft models that are molecularly characterized will enable both of these concepts to be further explored.

Supplementary Material

Refer to Web version on PubMed Central for supplementary material.

Acknowledgements

We thank R. Wilson for technical support and all other lab members for helpful discussion. This research is partially supported by grants to LX from Rally Foundation and Children's Cancer Fund (Dallas), to SXS from the Cancer Prevention and Research Institute of Texas (RP180319), and to YZ from Hyundai Hope on Wheels Foundation and Andrew McDonough B+ Foundation. Access to tissue biospecimens and bioinformatics support was facilitated by the UTSW Harold C. Simmons Comprehensive Cancer Center, supported by the National Cancer Institute (CA142543).

We acknowledge financial support from Rally Foundation and Children's Cancer Fund (Dallas), from the Cancer Prevention and Research Institute of Texas (RP180319), from Hyundai Hope on Wheels Foundation, from Andrew McDonough B+ Foundation and from the UTSW Harold C. Simmons Comprehensive Cancer Center, supported by the National Cancer Institute (CA142543).

References

1. Saab R, Spunt SL, Skapek SX. Myogenesis and rhabdomyosarcoma the Jekyll and Hyde of skeletal muscle. Curr Top Dev Biol 2011;94:197–234. [PubMed: 21295688]
2. Skapek SX, Ferrari A, Gupta AA, Lupo PJ, Butler E, Shipley J, et al. Rhabdomyosarcoma. Nat Rev Dis Primers 2019;5(1):1. [PubMed: 30617281]

3. Wang C Childhood rhabdomyosarcoma: recent advances and prospective views. J Dent Res 2012;91(4):341–50. [PubMed: 21917598]
4. Ognjanovic S, Linabery AM, Charbonneau B, Ross JA. Trends in childhood rhabdomyosarcoma incidence and survival in the United States, 1975-2005. Cancer 2009;115(18):4218–26. [PubMed: 19536876]
5. Martins AS, Olmos D, Missiaglia E, Shipley J. Targeting the insulin-like growth factor pathway in rhabdomyosarcomas: rationale and future perspectives. Sarcoma 2011;2011:209736. [PubMed: 21437217]
6. Parham DM, Qualman SJ, Teot L, Barr FG, Morotti R, Sorensen PH, et al. Correlation between histology and PAX/FKHR fusion status in alveolar rhabdomyosarcoma: a report from the Children's Oncology Group. Am J Surg Pathol 2007;31(6):895–901. [PubMed: 17527077]
7. Chen X, Stewart E, Shelat AA, Qu C, Bahrami A, Hatley M, et al. Targeting oxidative stress in embryonal rhabdomyosarcoma. Cancer Cell 2013;24(6):710–24. [PubMed: 24332040]
8. Shern JF, Chen L, Chmielecki J, Wei JS, Patidar R, Rosenberg M, et al. Comprehensive genomic analysis of rhabdomyosarcoma reveals a landscape of alterations affecting a common genetic axis in fusion-positive and fusion-negative tumors. Cancer Discov 2014;4(2):216–31. [PubMed: 24436047]
9. Seki M, Nishimura R, Yoshida K, Shimamura T, Shiraishi Y, Sato Y, et al. Integrated genetic and epigenetic analysis defines novel molecular subgroups in rhabdomyosarcoma. Nat Commun 2015;6:7557. [PubMed: 26138366]
10. Xu L, Zheng Y, Liu J, Rakheja D, Singleterry S, Laetsch TW, et al. Integrative Bayesian Analysis Identifies Rhabdomyosarcoma Disease Genes. Cell Rep 2018;24(1):238–51. [PubMed: 29972784]
11. Kas K, Voz ML, Roijer E, Astrom AK, Meyen E, Stenman G, et al. Promoter swapping between the genes for a novel zinc finger protein and beta-catenin in pleiomorphic adenomas with t(3;8)(p21;q12) translocations. Nat Genet 1997;15(2):170–4. [PubMed: 9020842]
12. Astrom A, D'Amore ES, Sainati L, Panarello C, Morerio C, Mark J, et al. Evidence of involvement of the PLAG1 gene in lipoblastomas. Int J Oncol 2000;16(6):1107–10. [PubMed: 10811981]
13. Zatkova A, Rouillard JM, Hartmann W, Lamb BJ, Kuick R, Eckart M, et al. Amplification and overexpression of the IGF2 regulator PLAG1 in hepatoblastoma. Gene Chromosome Canc 2004;39(2):126–37.
14. Landrette SF, Kuo YH, Hensen K, Barjesteh van Waalwijk van Doorn-Khosrovani S, Perrat PN, Van de Ven WJ, et al. Plag1 and Plagl2 are oncogenes that induce acute myeloid leukemia in cooperation with Cbfb-MYH11. Blood 2005;105(7):2900–7. [PubMed: 15585652]
15. Chen KS, Stroup EK, Budhipramono A, Rakheja D, Nichols-Vinueza D, Xu L, et al. Mutations in microRNA processing genes in Wilms tumors derepress the IGF2 regulator PLAG1. Genes Dev 2018;32(15-16):996–1007. [PubMed: 30026293]
16. Voz ML, Astrom AK, Kas K, Mark J, Stenman G, Van de Ven WJ. The recurrent translocation t(5;8)(p13;q12) in pleomorphic adenomas results in upregulation of PLAG1 gene expression under control of the LIFR promoter. Oncogene 1998;16(11):1409–16. [PubMed: 9525740]
17. Astrom AK, Voz ML, Kas K, Roijer E, Wedell B, Mandahl N, et al. Conserved mechanism of PLAG1 activation in salivary gland tumors with and without chromosome 8q12 abnormalities: identification of SII as a new fusion partner gene. Cancer Res 1999;59(4):918–23. [PubMed: 10029085]
18. Hibbard MK, Kozakewich HP, Dal Cin P, Sciot R, Tan X, Xiao S, et al. PLAG1 fusion oncogenes in lipoblastoma. Cancer Res 2000;60(17):4869–72. [PubMed: 10987300]
19. Voz ML, Agten NS, Van de Ven WJ, Kas K. PLAG1, the main translocation target in pleomorphic adenoma of the salivary glands, is a positive regulator of IGF-II. Cancer Res 2000;60(1):106–13. [PubMed: 10646861]
20. Voz ML, Mathys J, Hensen K, Pendeville H, Van Valckenborgh I, Van Huffel C, et al. Microarray screening for target genes of the proto-oncogene PLAG1. Oncogene 2004;23(1):179–91. [PubMed: 14712223]
21. Hensen K, Braem C, Declercq J, Van Dyck F, Dewerchin M, Fiette L, et al. Targeted disruption of the murine Plag1 proto-oncogene causes growth retardation and reduced fertility. Dev Growth Differ 2004;46(5):459–70. [PubMed: 15606491]

22. DeChiara TM, Efstratiadis A, Robertson EJ. A growth-deficiency phenotype in heterozygous mice carrying an insulin-like growth factor II gene disrupted by targeting. Nature 1990;345(6270):78–80. [PubMed: 2330056]
23. Queimado L, Lopes C, Du F, Martins C, Bowcock AM, Soares J, et al. Pleomorphic adenoma gene 1 is expressed in cultured benign and malignant salivary gland tumor cells. Lab Invest 1999;79(5):583–9. [PubMed: 10334569]
24. El-Badry OM, Minniti C, Kohn EC, Houghton PJ, Daughaday WH, Helman LJ. Insulin-like growth factor II acts as an autocrine growth and motility factor in human rhabdomyosarcoma tumors. Cell Growth Differ 1990;1(7):325–31. [PubMed: 2177632]
25. Zhan S, Shapiro DN, Helman LJ. Activation of an imprinted allele of the insulin-like growth factor II gene implicated in rhabdomyosarcoma. J Clin Invest 1994;94(1):445–8. [PubMed: 8040287]
26. Zheng Y, Devitt C, Liu J, Iqbal N, Skapek SX. Arf induction by Tgfbeta is influenced by Sp1 and C/ebpbeta in opposing directions. PLoS One 2013;8(8):e70371. [PubMed: 23940569]
27. Zheng Y, Zhao YD, Gibbons M, Abramova T, Chu PY, Ash JD, et al. Tgfbeta signaling directly induces Arf promoter remodeling by a mechanism involving Smads 2/3 and p38 MAPK. J Biol Chem 2010;285(46):35654–64. [PubMed: 20826783]
28. Silva RL, Thornton JD, Martin AC, Rehg JE, Bertwistle D, Zindy F, et al. Arf-dependent regulation of Pdgf signaling in perivascular cells in the developing mouse eye. EMBO J 2005;24(15):2803–14. [PubMed: 16037818]
29. Zheng Y, Devitt C, Liu J, Mei J, Skapek SX. A distant, cis-acting enhancer drives induction of Arf by Tgfbeta in the developing eye. Dev Biol 2013;380(1):49–57. [PubMed: 23665474]
30. McKeller RN, Fowler JL, Cunningham JJ, Warner N, Smeyne RJ, Zindy F, et al. The Arf tumor suppressor gene promotes hyaloid vascular regression during mouse eye development. Proc Natl Acad Sci U S A 2002;99(6):3848–53. [PubMed: 11891301]
31. Burns JL, Hassan AB. Cell survival and proliferation are modified by insulin-like growth factor 2 between days 9 and 10 of mouse gestation. Development 2001;128(19):3819–30. [PubMed: 11585807]
32. White MF. Regulating insulin signaling and beta-cell function through IRS proteins. Can J Physiol Pharmacol 2006;84(7):725–37. [PubMed: 16998536]
33. Chao W, D'Amore PA. IGF2: epigenetic regulation and role in development and disease. Cytokine Growth Factor Rev 2008;19(2):111–20. [PubMed: 18308616]
34. Wittman MD, Carboni JM, Yang Z, Lee FY, Antman M, Attar R, et al. Discovery of a 2,4-disubstituted pyrrolo[1,2-f][1,2,4]triazine inhibitor (BMS-754807) of insulin-like growth factor receptor (IGF-1R) kinase in clinical development. J Med Chem 2009;52(23):7360–3. [PubMed: 19778024]
35. Skapek SX, Anderson J, Barr FG, Bridge JA, Gastier-Foster JM, Parham DM, et al. PAX-FOXO1 fusion status drives unfavorable outcome for children with rhabdomyosarcoma: a children's oncology group report. Pediatr Blood Cancer 2013;60(9):1411–7. [PubMed: 23526739]
36. Tollefsen SE, Sadow JL, Rotwein P. Coordinate expression of insulin-like growth factor II and its receptor during muscle differentiation. Proc Natl Acad Sci U S A 1989;86(5):1543–7. [PubMed: 2537977]
37. Tollefsen SE, Lajara R, McCusker RH, Clemmons DR, Rotwein P. Insulin-like growth factors (IGF) in muscle development. Expression of IGF-I, the IGF-I receptor, and an IGF binding protein during myoblast differentiation. J Biol Chem 1989;264(23):13810–7. [PubMed: 2474537]
38. Stewart CE, James PL, Fant ME, Rotwein P. Overexpression of insulin-like growth factor-II induces accelerated myoblast differentiation. J Cell Physiol 1996;169(1):23–32. [PubMed: 8841419]
39. Coleman ME, DeMayo F, Yin KC, Lee HM, Geske R, Montgomery C, et al. Myogenic vector expression of insulin-like growth factor I stimulates muscle cell differentiation and myofiber hypertrophy in transgenic mice. J Biol Chem 1995;270(20):12109–16. [PubMed: 7744859]
40. Liu JP, Baker J, Perkins AS, Robertson EJ, Efstratiadis A. Mice carrying null mutations of the genes encoding insulin-like growth factor I (Igf-1) and type 1 IGF receptor (Igf1r). Cell 1993;75(1):59–72. [PubMed: 8402901]

41. Ruijtenberg S, van den Heuvel S. Coordinating cell proliferation and differentiation: Antagonism between cell cycle regulators and cell type-specific gene expression. Cell Cycle 2016;15(2):196–212. [PubMed: 26825227]

42. Ren H, Accili D, Duan C. Hypoxia converts the myogenic action of insulin-like growth factors into mitogenic action by differentially regulating multiple signaling pathways. Proc Natl Acad Sci U S A 2010;107(13):5857–62. [PubMed: 20231451]

43. Nguyen TH, Barr FG. Therapeutic Approaches Targeting PAX3-FOXO1 and Its Regulatory and Transcriptional Pathways in Rhabdomyosarcoma. Molecules 2018;23(11).

44. Wan X, Harkavy B, Shen N, Grohar P, Helman LJ. Rapamycin induces feedback activation of Akt signaling through an IGF-1R-dependent mechanism. Oncogene 2007;26(13):1932–40. [PubMed: 17001314]

45. Wan X, Helman LJ. Effect of insulin-like growth factor II on protecting myoblast cells against cisplatin-induced apoptosis through p70 S6 kinase pathway. Neoplasia 2002;4(5):400–8. [PubMed: 12192598]

46. Doros L, Yang J, Dehner L, Rossi CT, Skiver K, Jarzembowski JA, et al. DICER1 mutations in embryonal rhabdomyosarcomas from children with and without familial PPB-tumor predisposition syndrome. Pediatr Blood Cancer 2012;59(3):558–60. [PubMed: 22180160]

47. Weigel B, Malempati S, Reid JM, Voss SD, Cho SY, Chen HX, et al. Phase 2 trial of cixutumumab in children, adolescents, and young adults with refractory solid tumors: a report from the Children's Oncology Group. Pediatr Blood Cancer 2014;61(3):452–6. [PubMed: 23956055]

48. Pappo AS, Vassal G, Crowley JJ, Bolejack V, Hogendoorn PC, Chugh R, et al. A phase 2 trial of R1507, a monoclonal antibody to the insulin-like growth factor-1 receptor (IGF-1R), in patients with recurrent or refractory rhabdomyosarcoma, osteosarcoma, synovial sarcoma, and other soft tissue sarcomas: results of a Sarcoma Alliance for Research Through Collaboration study. Cancer 2014;120(16):2448–56. [PubMed: 24797726]

49. Wagner LM, Fouladi M, Ahmed A, Krailo MD, Weigel B, DuBois SG, et al. Phase II study of cixutumumab in combination with temsirolimus in pediatric patients and young adults with recurrent or refractory sarcoma: a report from the Children's Oncology Group. Pediatr Blood Cancer 2015;62(3):440–4. [PubMed: 25446280]

50. Kolb EA, Gorlick R, Maris JM, Keir ST, Morton CL, Wu J, et al. Combination testing (Stage 2) of the Anti-IGF-1 receptor antibody IMC-A12 with rapamycin by the pediatric preclinical testing program. Pediatr Blood Cancer 2012;58(5):729–35. [PubMed: 21630428]

51. Houghton PJ, Morton CL, Gorlick R, Kolb EA, Keir ST, Reynolds CP, et al. Initial testing of a monoclonal antibody (IMC-A12) against IGF-1R by the Pediatric Preclinical Testing Program. Pediatr Blood Cancer 2010;54(7):921–6. [PubMed: 20166202]

52. Van Dyck F, Declercq J, Braem CV, Van de Ven WJ. PLAG1, the prototype of the PLAG gene family: versatility in tumour development (review). Int J Oncol 2007;30(4):765–74. [PubMed: 17332914]

Implications:

Our data demonstrate that PLAG1 contributes to proliferation and survival of RMS cells at least partially by inducing IGF2, and this new understanding may have the potential for clinical translation.

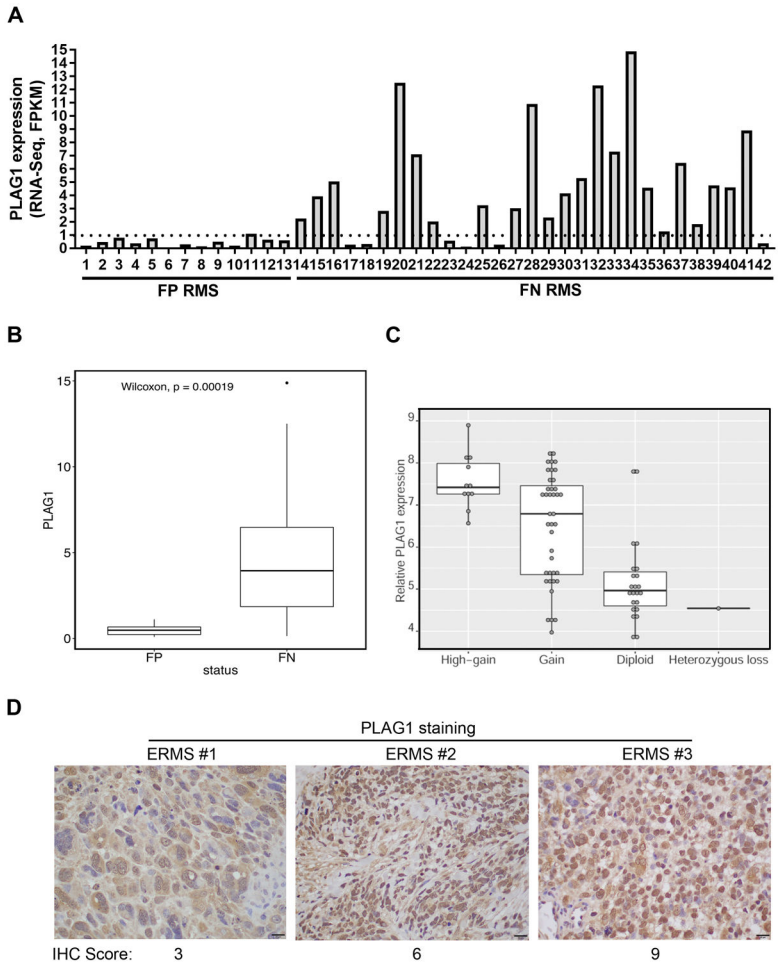

Figure 1. Aberrant expression of PLAG1 in RMS.

A. Chart shows mRNA expression of PLAG1 in 42 RMS specimens. Data are from RNA-Seq studies and are expressed as FPKM (Fragments Per Kilobase of transcript per Million mapped reads). B. Plot shows PLAG1 expression level is significantly higher in fusion-negative (FN) RMS specimens than that of fusion-positive (FP) RMS specimens. C. Plot displays PLAG1 expression in RMS specimens correlates with copy number (CN) gain. x-axis is for copy-number status of PLAG1 gene only, which is in comparison to reference human genome. Two to three copies of DNA is defined as CN gain and more than three copies as high-gain. D. Representative photomicrographs of immunohistochemistry stained (for PLAG1) slides of three ERMS specimens. The IHC score (range from 0 to 9, see Methods for details) is shown under each photomicrograph. Scale bar is for 20 μm.

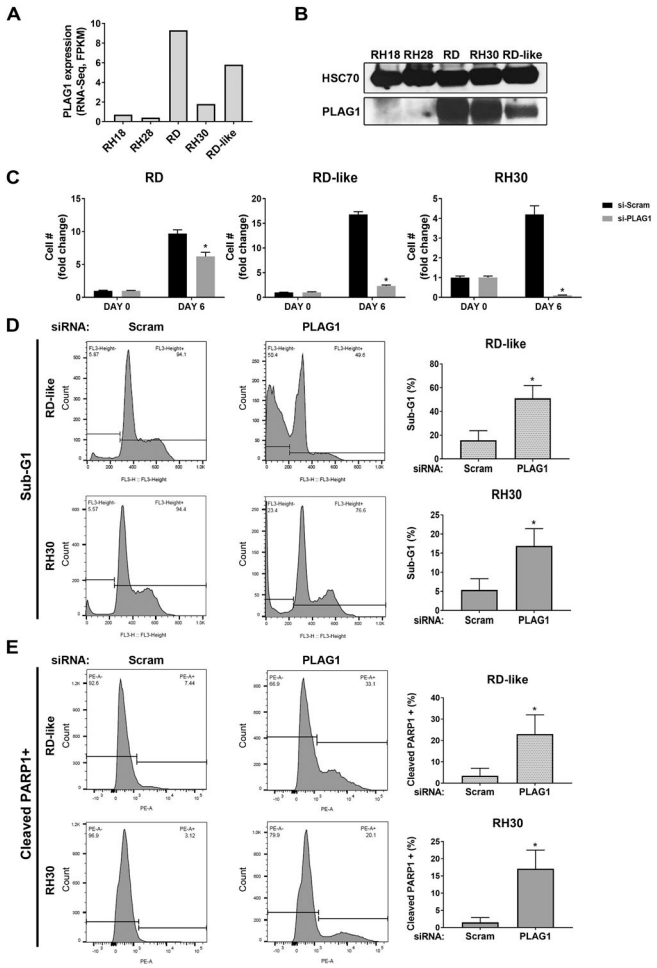

Figure 2. Knockdown of PLAG1 impairs cell accumulation and induces apoptosis in RMS cells.

A. Chart shows mRNA expression of PLAG1 in five RMS cell lines. Data are from RNA-Seq studies and are expressed as FPKM. B. Representative immunoblot shows that expression PLAG1 protein in five RMS cell lines. HSC70 serves as loading control. C. Charts demonstrate that knockdown of PLAG1 significantly decreases cell accumulation in RD, RD-like, and RH30 cells. Data are shown as fold change of day 6 versus day 0. Asterisks indicate p value < 0.05 by two-tailed Student's t test. D and E. Representative charts demonstrate that knockdown of PLAG1 increases the number of cells in sub-G1 phase (D) and induces cleaved-PARP1 (E) in RD-like and RH30 cells (left two panels). Quantitative data are displayed as average and standard deviation derived from three experiments (right panel). Asterisks indicate p value < 0.05 by two-tailed Student's t test.

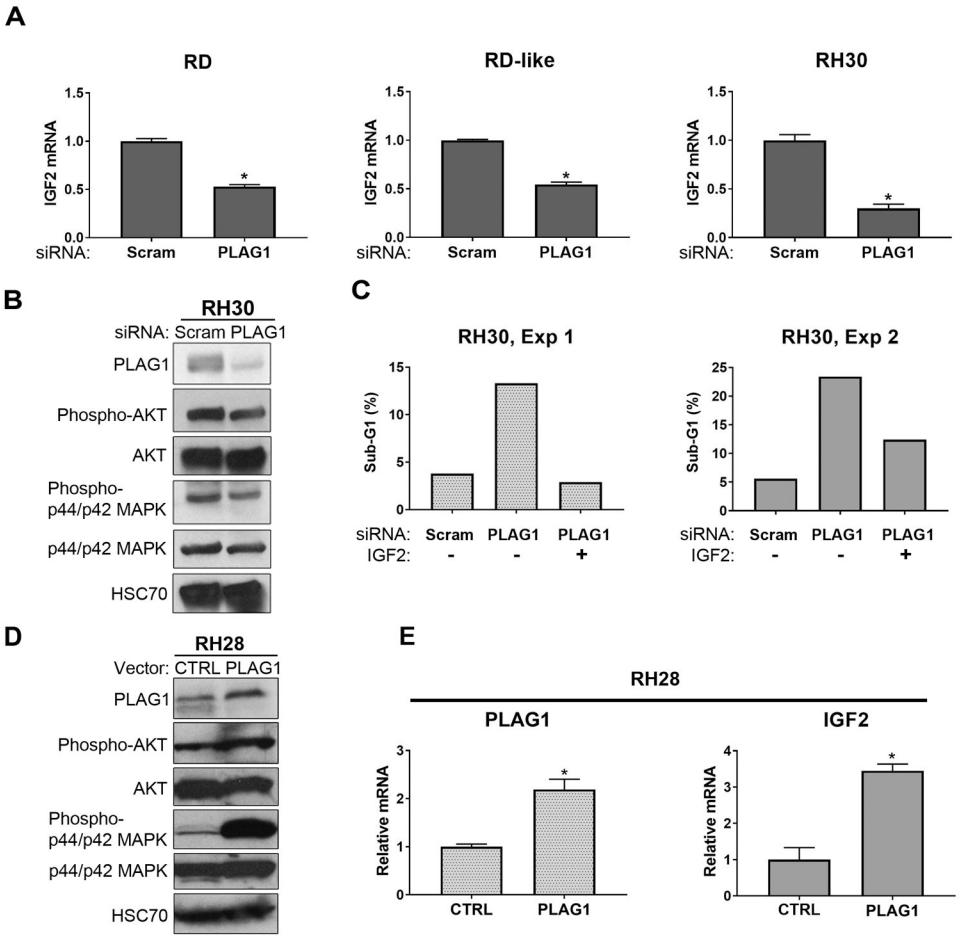

Figure 3. PLAG1 controls IGF2 expression and its downstream signaling.

A. Real-time qRT-PCR demonstrates that knockdown of PLAG1 significantly decreases IGF2 mRNA expression in RD, RD-like and RH30 cells. Expression is relative to *GAPDH*, and data are displayed as average and standard deviation derived from two experiments. Asterisks indicate p value < 0.05 by two-tailed Student's t test. B. Representative western blot shows the expression of PLAG1, phospho-AKT, AKT, phospho-p44/p42 MAPK, p44/p42 MAPK and HSC70 (loading control) from RH30 cells upon treated with scramble (Scram) siRNA or siRNA targeting PLAG1. C. Representative charts demonstrate that addition of IGF2 reduces the sub-G1 population induced by PLAG knockdown in RH30 cells (data from two experiments are displayed separately). D. Representative western blot shows the expression of PLAG1, phospho-AKT, AKT, phospho-p44/p42 MAPK, p44/p42 MAPK, and HSC70 (loading control) from RH28 cells with ectopic expression of PLAG1. E. Real-time qRT-PCR demonstrates that ectopic expression of PLAG1 significantly increases IGF2 expression in RH28 cells. mRNA expression is relative to *GAPDH*, and data are displayed as average and standard deviation derived from two experiments. Asterisks indicate p value < 0.05 by two-tailed Student's t test.

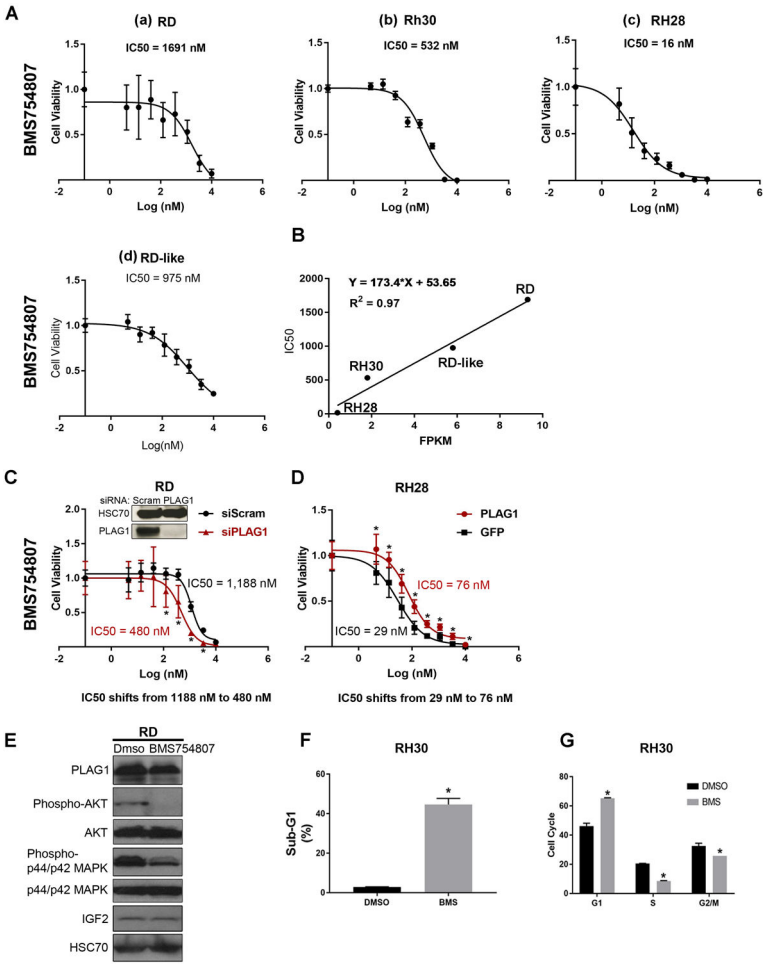

Figure 4. PLAG1 expression level is a biomarker of resistance to inhibitor of IGF signaling.

A. Charts show IC50 of BMS754807 in RD (a), RH30 (b), RH28 (c), and RD-like (d) cells. IC50 of BMS754807 is determined by GraphPad Prism7 software. B. Chart displays the correlation between IC50 of BMS754807 and PLAG1 expression level (RNA-Seq, FPKM) in RMS cells. C and D. Chart displays the dose responsive curve of BMS754807 in RD cells treated with indicated siRNA (C) or RH28 cells transduced with retrovirus expressing GFP control or PLAG1 (D). IC50 of BMS754807 was determined by GraphPad Prism7 software. Two-tailed Student's t test was used to compare each data point. Asterisks indicate p value < 0.05. E. Representative western blot shows the expression of PLAG1, phospho-AKT, AKT, phospho-p44/p42 MAPK, p44/p42 MAPK, IGF2 and HSC70 (loading control) from RD cells upon treated with control DMSO or BMS754807 (2 μM) for 72 hours. F and G. Charts demonstrate that BMS754807 (2 μM) treatment for 72 hours significantly increases the number of cells in sub-G_1 phase (F) and induces cell cycle arrest at G_1, G_2/M phase and decreases the number of cell in S phase (G) of RH30 cells. Quantitative data are displayed as average and standard deviation derived from two experiments. Asterisks indicate p value < 0.05 by two-tailed Student's t test.

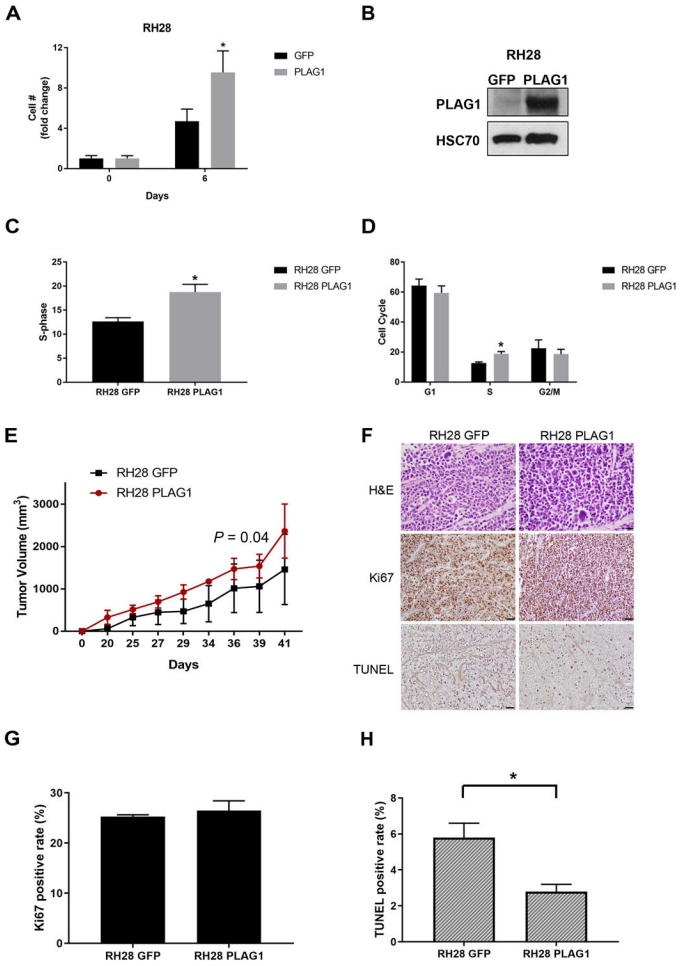

Figure 5. Ectopic expression of PLAG1 drives cell proliferation and tumor growth.

A. Chart displays the number of RH28 cells, assessed by Cy-QUANT, on the indicated days of *in vitro* propagation. Cells were transduced with retroviral vectors encoding GFP (control) or PLAG1 prior to plating. Quantitative data displayed as average and standard deviation, are derived from multiple biological replicates (n=36). Asterisks represent p value < 0.05 by two-tailed Student's t test. B. Representative western blot shows the expression of PLAG1 and HSC70 (loading control) from RH28 cells upon transduced with retroviral vectors encoding GFP (control) or PLAG1. C and D. Charts display the distribution of G1, S and G2/M phase of RH28 cells after transduced with retroviral vectors encoding GFP (control) or PLAG1. Quantitative data, displayed as average and standard deviation, are derived from two experiments. Asterisks represent p value < 0.05 by two-tailed Student's t test. Chart in C only displays the cells in S phase. E. Plot displays tumor volume of individual xenografts formed by RH28 cells, transduced with lentiviral vectors encoding GFP (control) or PLAG1, prior to subcutaneous implantation. All tumors were harvested when experimental tumors reached an average tumor size of 2.0 cm^3. Differences in tumor volume are statistically significant (P = 0.04, Two-way ANOVA test). F. Representative photomicrographs of hematoxylin- and eosin- stained (upper panels), Ki67 stained (middle panels), and TUNEL stained (bottom panels) slides of RH28 xenografts described in E. Scale bar is for 20 μm. G and H. Quantitative analysis shows average percentage and

standard deviation of Ki67 (G) and TUNEL (H) -positive cells within tumor sections of RH28 GFP and RH28 PLAG1 as shown in F. Asterisks represent p value < 0.05 by two-tailed Student's t test.